# Superresolution digital holographic microscopy for three-dimensional samples

**Vicente Micó[1*], Zeev Zalevsky[2], Carlos Ferreira[1], and Javier García[1]**

[1]*Departamento de Óptica, Universitat de Valencia, C/Dr. Moliner, 50, 46100 Burjassot, Spain*
[2]*School of Engineering, Bar-Ilan University, Ramat-Gan, 52900 Israel*
[*]*Corresponding author: vicente.mico@uv.es*

**Abstract:** An approach that allows superresolution imaging of three-dimensional (3-D) samples by numerical refocusing is presented in the field of digital holographic microscopy. Based on the object's spectrum shift produced by tilted illumination, we present a time multiplexing superresolved approach to overcome the Abbe's diffraction limit. The proposed approach uses a microscope in a Mach-Zehnder interferometric architecture with the particularity that the output plane does not coincide with the image plane. Thus, a set of off-axis non-image plane holograms are sequentially recorded for every tilted beam used in the illumination stage. After that and by using simple digital post-processing and numerical reconstruction, a 3-D superresolved sample volume is reconstructed slice-by-slice in terms of the definition of a synthetic aperture (SA) that expands the cutoff frequency of the microscope lens. Experimental results showing the capabilities of the proposed approach are presented.



**OCIS codes**: (100.6640) Superresolution; (100.6890) Three-dimensional image processing; (110.0180) Microscopy; (090.1995) Digital holography

## References and links

1. J. W. Goodman and R. W. Lawrence, "Digital Image Formation from Electronically Detected Holograms," Appl. Phys. Lett. **11**, 77-79 (1967).
2. U. Schnars and W. P. Jueptner, *Digital Holography*, (Springer, 2005).
3. T. Kreis, *Hankbook of holographic interferometry: optical and digital methods* (Wiley-VCH, 2005).
4. L. P. Yaroslavsky, *Digital Holography and Digital Image Processing: Principles, Methods, Algorithms* (Kluwer, 2003).
5. L. Yu and M. K. Kim, "Wavelength-scanning digital interference holography for tomographic 3D imaging using the angular spectrum method," Opt. Lett. **30**, 2092-2094 (2005).
6. G. Pedrini, P. Froning, H. Tiziani, and F. Santoyo, "Shape measurement of microscopic structures using digital holograms," Opt. Commun. **164**, 257-268 (1999).
7. E. Cuche, F. Bevilacqua, and Ch. Depeursinge, "Digital holography for quantitative phase-contrast imaging," Opt. Lett. **24**, 291-293 (1999).
8. C. Wagner, W. Osten, and S. Seebacher, "Direct shape measurement by digital wavefront reconstruction and multiwavelength contouring," Opt. Eng. **39**, 79-85 (2000)
9. S. Murata and N. Yasuda, "Potential of digital holography in particle measurements," Opt. Laser Technol. **32**, 567-574 (2000).
10. A. Stadelmaier and J. H. Massig, "Compensation of lens aberrations in digital holography," Opt. Lett. **25**, 1630–1632 (2000).
11. B. W. Schilling, T.-Ch. Poon, G. Indebetouw, B. Storrie, K. Shinoda, Y. Suzuki, and M. H. Wu, "Three-dimensional holographic fluorescence microscopy," Opt. Lett. **22**, 1506-1508 (1997).
12. E. Cuche, P. Marquet, and Ch. Depeursinge, "Simultaneous amplitude-contrast and quantitative phase-contrast microscopy by numerical reconstruction of Fresnel off-axis holograms," Appl. Opt. **38**, 6994-7001 (1999).
13. F. Dubois, L. Joannes, and J.-C. Legros, "Improved three-dimensional imaging with a digital holographic microscope with a source of partial spatial coherence," Appl. Opt. **38**, 7085-7094 (1999).
14. P. Marquet, B. Rappaz, P. J. Magistretti, E. Cuche, Y. Emery, T. Colomb, and Ch. Depeursinge, "Digital holographic microscopy: a noninvasive contrast imaging technique allowing quantitative visualization of living cells with subwavelength axial accuracy," Opt. Lett. **30**, 468-470 (2005).

#99857 - $15.00 USD Received 5 Aug 2008; revised 15 Sep 2008; accepted 22 Sep 2008; published 6 Nov 2008

15. P. Ferraro, D. Alferi, S. De Nicola, L. De Petrocellis, A. Finizio, and G. Pierattini, "Quantitative phase-contrast microscopy by a lateral shear approach to digital holographic image reconstruction," Opt. Lett. **31**, 1405-1407 (2006).
16. T. Colomb, F. Dürr, E. Cuche, P. Marquet, H. G. Limberger, R.-P. Salathé, and Ch. Depeursinge, "Polarization microscopy by use of digital holography: application to optical-fiber birefringence measurements," Appl. Opt. **44**, 4461-4469 (2005).
17. P. Ferraro, S. De Nicola, A. Finizio, G. Coppola, S. Grilli, C. Magro, and G. Pierattini, "Compensation of the Inherent Wave Front Curvature in Digital Holographic Coherent Microscopy for Quantitative Phase-Contrast Imaging," Appl. Opt. **42**, 1938-1946 (2003).
18. T. Colomb, E. Cuche, F. Charrière, J. Kühn, N. Aspert, F. Montfort, P. Marquet, and Ch. Depeursinge, "Automatic procedure for aberration compensation in digital holographic microscopy and applications to specimen shape compensation," Appl. Opt. **45**, 851–863 (2006).
19. J. Sheng, E. Malkiel, and J. Katz, "Digital holographic microscope for measuring three-dimensional particle distributions and motions," Appl. Opt. **45**, 3893-3901 (2006).
20. P. Ferraro, S. Grilli, D. Alfieri, S. De Nicola, A. Finizio, G. Pierattini, B. Javidi, G. Coppola, and V. Striano, "Extended focused image in microscopy by digital holography," Opt. Express **13**, 6738-6749 (2005).
21. F. Dubois, C. Yourassowsky, O. Monnom, J.-C. Legros, O. Debeir, P. Van Ham, R. Kiss, and Ch. Decaestecker, "Digital holographic microscopy for the three-dimensional dynamic analysis of in vitro cancer cell migration," J. Biomed. Opt. **11**, 054032 (2006).
22. D. Gabor, "A new microscopic principle," Nature **161**, 777-778 (1948).
23. E. N. Leith and J. Upatnieks, "Reconstructed wavefronts and communication theory," J. Opt. Soc. Am. **52**, 1123-1130 (1962).
24. E. N. Leith and J. Upatnieks, "Wavefront reconstruction with continuous-tone objects," J. Opt. Soc. Am. **53**, 1377-1381 (1963).
25. E. N. Leith and J. Upatnieks, "Wavefront reconstruction with diffuse illumination and three-dimensional objects," J. Opt. Soc. Am. **54**, 1295-1301 (1964).
26. W. Xu, M. H. Jericho, I. A. Meinertzhagen, and H. J. Kreuzer, "Digital In-line Holography for Biological Applications," Proc. Natl. Acad. Sci. USA **98**, 11301-11305 (2001).
27. J. Garcia-Sucerquia, W. Xu, S. K. Jericho, P. Klages, M. H. Jericho, and H. J. Kreuzer, "Digital in-line holographic microscopy," Appl. Opt. **45**, 836-850 (2006).
28. J. Garcia-Sucerquia, W. Xu, M. H. Jericho, and H. J. Kreuzer, "Immersion digital in-line holographic microscopy," Opt. Lett. **31**, 1211-1213 (2006).
29. C. J. Schwarz, Y. Kuznetsova and S. R. J. Brueck, "Imaging interferometric microscopy," Opt. Lett. **28**, 1424-1426 (2003).
30. V. Mico, Z. Zalevsky, P. García-Martínez, and J. García, "Superresolved imaging in digital holography by superposition of tilted wavefronts," Appl. Opt. **45**, 822-828 (2006).
31. V. Mico, Z. Zalevsky, and J. García, "Superresolution Optical System by Common-Path Interferometry," Opt. Express **14**, 5168-5177 (2006).
32. V. Mico, Z. Zalevsky, P. García-Martínez, and J. García, "Synthetic Aperture Superresolution Using Multiple Off-axis Holograms," J. Opt. Soc. Am. A **23**, 3162-3170 (2006).
33. Y. Kuznetsova, A. Neumann, and S. R. J. Brueck, "Imaging interferometric microscopy – approaching the linear systems limits of optical resolution," Opt. Express **15**, 6651-6663 (2007).
34. J. R. Price, P. R. Bingham, and C. E. Thomas Jr, "Improving resolution in microscopic holography by computationally fusing multiple, obliquely illuminated object waves in the Fourier domain," Appl. Opt. **46**, 826-833 (2007).
35. G. Indebetouw, Y. Tada, J. Rosen, and G. Brooker, "Scanning holographic microscopy with resolution exceeding the Rayleigh limit of the objective by superposition of off-axis holograms," Appl. Opt. **46**, 993-1000 (2007).
36. V. Mico, Z. Zalevsky, and J. García, "Synthetic aperture microscopy using off-axis illumination and polarization coding," Opt. Commun. **276**, 209-217 (2007).
37. V. Mico, Z. Zalevsky, and J. García, "Common-path phase-shifting digital holographic microscopy: a way to quantitative phase imaging and superresolution," Opt. Commun. **281**, 4273-4281 (2008).
38. A. Neumann, Y. Kuznetsova, and S. R. Brueck, "Structured illumination for the extension of imaging interferometric microscopy," Opt. Express **16**, 6785-6793 (2008).
39. D. Mas, J. Garcia, C. Ferreira, L. M. Bernardo, and F. Marinho, "Fast algorithms for free-space diffraction patterns calculation," Opt. Commun. **164**, 233-245 (1999).

## 1. Introduction

Since it was first proposed by Goodman and Lawrence more than 40 years ago [1], digital holography appears as a powerful tool for a wide range of different applications [2,3]. Digital

#99857 - $15.00 USD Received 5 Aug 2008; revised 15 Sep 2008; accepted 22 Sep 2008; published 6 Nov 2008

holography takes the basics of classical holography concerning whole 3-D information (complex amplitude distribution) of the object wavefront but with the advantages of digital processing methods provided by computers [4,5]. Aside of a long and rich history in other fields [6-10], digital holography is combined with microscopy to avoid the limited depth of focus in high NA lenses and the high magnification ratios needed in conventional optical microscope imaging. Moreover, digital holographic microscopy (DHM) allows 3-D sample imaging by numerical refocusing of a two-dimensional (2-D) image at different object planes without using any opto-mechanical movement [11-13]. Due to its versatility, DHM is applied to real-time quantitative phase contrast imaging [14,15], polarization microscopy imaging [16], aberration lens compensation [17,18], particle tracking [19], extended depth of focus imaging [20], 3-D dynamic analysis of cells [21] and so on.

Recently, the original principle proposed by Gabor in 1948 [22] and extended by Leith and Upatnieks some years later [23-25] is causing a strong interest because of its extremely simple experimental configuration. Digital in-line holography with spherical waves is the simplest realization of the digital holographic method as it works without lenses [26,27]. However, digital in-line holography still presents a limited depth of field with an elongated depth of focus [19] and it requires complex procedures such as sample immersion in a high refractive index medium to achieve high-resolution imaging [28].

On the other hand, superresolution imaging using tilted wave illumination [29-38] has been experimentally demonstrated in DHM as a successful method to improve the limited resolution of microscope lenses beyond the Abbe's diffraction limit. In some cases [30-32,36,37], superresolved DHM is applied to low NA lenses in order to achieve medium and high resolution imaging while maintaining the highly attractive properties concerning a low NA microscope objective, that is, long working distance, large field of view, large depth of focus and low cost. In other cases [29,33-35,38], the use of medium and/or high NA lenses in combination with tilted illumination allow the definition of a resolution limit that approaches the theoretical diffraction limit. But in all the cases, the experimental arrangement is based on an interferometric image plane recording to recover the transmitted frequency band-pass selected by the tilted illumination. Finally, a SA is assembled in a latter stage.

In this paper, we present for the first time a combination of techniques that enables full 3-D superresolution imaging over the whole volume of the input sample. It is based on the off-axis holographic recording of a non-focused image of the sample produced when a given light beam illuminates the sample. Thus, it is possible to recover the additional spatial frequency information of the sample's spectrum contained in each elementary pupil that is obtained using on-axis and off-axis illumination beams in sequential mode. Moreover, because of the recording is performed by considering misfocused images, the dynamic range of the CCD camera becomes optimized, as high concentration of light associated with in focus objects is avoided. With this procedure, full 2-D frequency space coverage of the sample is achieved by time multiplexing both the illumination onto the sample and the recording process at the CCD plane. After that, digital post-processing enables the refocusing of the set of recovered frequency bands at different and arbitrary distances. This fact means that a SA can be generated for each one of the 2-D transversal reconstructed sections, or in other words, this numerical reconstruction allows the definition of a stack of slices of superresolved images that are refocused at incremental depths and that cover the whole sample volume. Experimental results are provided showing an experimental resolution improvement by a factor of 3 (the SA has tripled the cutoff frequency of the conventional one) when a 0.42NA long working distance infinity corrected microscope lens is used.

The paper is organized as follows. Section 2 provides a description of the optical experimental setup while Section 3 presents the considered methodology. Section 4 shows experimental results for swine sperm cells as input object and Section 5 concludes the paper.

## 2. Description of the optical setup.

The optical system setup used to test the capabilities of the proposed approach can be seen in Fig. 1. Light that is coming from a He-Ne laser is split by a first beam splitter ($BS_1$) allowing

#99857 - $15.00 USD Received 5 Aug 2008; revised 15 Sep 2008; accepted 22 Sep 2008; published 6 Nov 2008

the implementation of a basic Mach-Zehnder interferometric architecture. On one branch (*imaging branch*), we place a microscope setup in transmission mode. The microscope objective produces a magnified image of the transparent sample with the particularity that no particular sample plane is imaged on the CCD. Thus no specific part of the object is focussed on the CCD. This fact is accomplished by either moving back the CCD or moving forward the input sample. In any case, the transmitted object information of the recorded image is preserved despite of that slightl misfocus. Moreover, the missfocus spreads the light of the object over a large area, reducing the dynamic range needs for recording objects intensity and the corresponding hologram.

Under this condition, the CCD images a magnified wavefront coming from the image plane but not a focused image of the object itself. A second beam splitter ($BS_2$) allows the addition of a reference beam incoming from the second branch (*reference branch*) of the interferometric configuration. Thus, the CCD records a Fresnel hologram of the transmitted object wavefront with the particularity that the bending mirror of the reference branch is slightly tilted. So, the reference beam reaches the CCD at oblique incidence, that is, forming a small angle with the propagation direction of the object beam.

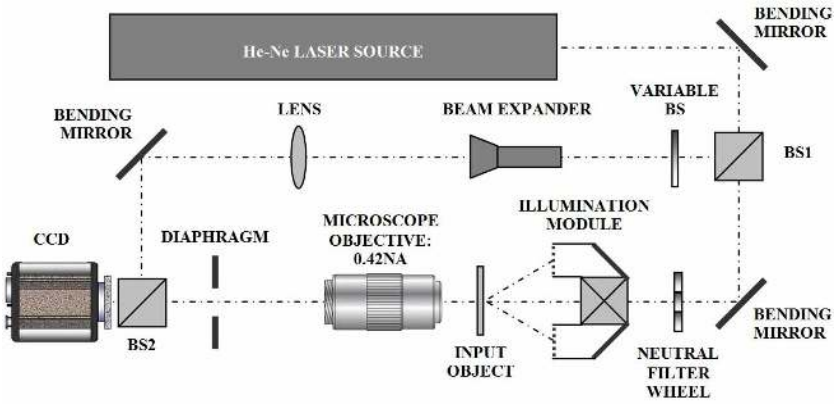


Fig. 1. Sketch of the experimental arrangement for 3-D superresolution imaging.

A lens in the reference branch allows divergence compensation between both interferometric beams. Thus, the recorded Fresnel hologram becomes equivalent to a lensless Fourier hologram where the exact Fourier transformation of the transmitted frequency band-pass is directly obtained if we perform a digital Fourier transformation of the recorded hologram. Additional optical elements such as neutral density filters, a beam expander and a diaphragm contribute to the optimization of the holographic recording process.

The previously described process is performed considering a set of tilted beams impinging onto the input object in sequential mode. In our experiment, we have used 8 off-axis beams aside the on-axis one, however, a different configuration can be defined as well. By properly matching the angle of the tilted beams with the NA of the microscope lens and the illumination wavelength that is used in the experiment, it is possible to transmit contiguous 2-D frequency bands of the object's spectrum. This fact allows the sequential transmission through the aperture of the microscope lens of a set of elementary pupils covering the full 2-D frequency space of the object's spectrum.

A picture of the experimental arrangement assembled at the laboratory is presented in Fig. 2(a) where the analogy with Fig. 1 identifies the different setup components. Tilted illumination is provided by an illumination module composed by a pair of mirrors at 45 degrees configuration and a holographically-recorded diffraction grating (named as *illumination grating*) which is mounted onto a rotatable holder [see Fig. 2(b)]. The mirrors move parallel to the optical axis the incoming laser beam and then a tilted beam illuminating the input sample is achieved considering the -1 diffraction order of the illumination grating.

#99857 - $15.00 USD Received 5 Aug 2008; revised 15 Sep 2008; accepted 22 Sep 2008; published 6 Nov 2008

Using this illumination assembly, different incidence directions for the oblique beams are sequentially lit by tilting the illumination assembly around the optical axis by using a rotatable holder. In our experiment, a 45º step is performed between subsequent oblique illuminations in such a way that full 2-D frequency space is covered using 8 positions at the illumination assembly. In addition, on-axis illumination is also produced by removing mirror 1 in Fig. 2(b).

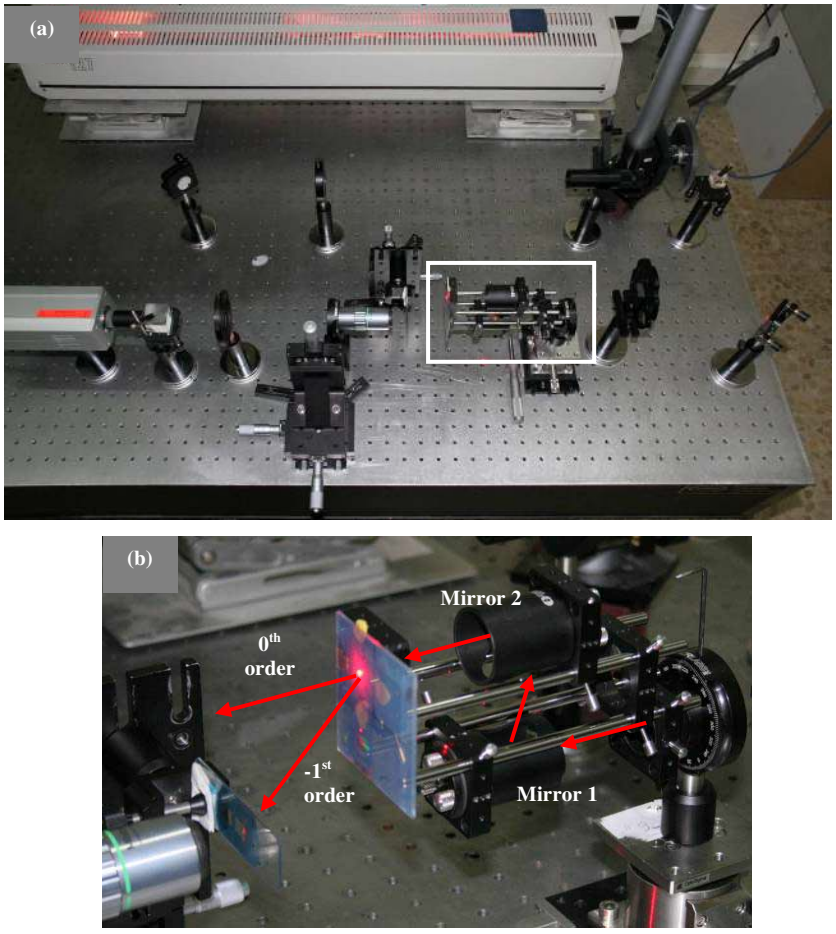


Fig. 2. Pictures of the experimental setup at the laboratory. Each optical element in case (a) can be identified from Fig. 1. Case (b) represents the magnified area corresponding with the white rectangle depicted in case (a).

## 3. Methodology.

Once the whole process is performed (we are time multiplexing the spatial information of the input object), a set of different holograms that were recorded in off-axis geometry is stored in the computer's memory. Then, it is possible to recover the complex amplitude distribution of the transmitted frequency band-pass by applying a Fourier transformation over the recorded holograms and considering the distribution located at one of the diffraction orders. After filtering and centering process, each recovered elementary pupil can be numerically processed in order to propagate them to different distances.

There are different numerical methods useful for digital reconstruction of the diffraction integral [2-5,39]. The diffraction Rayleigh-Sommerfeld integral can be approximately solved using either the Fresnel transformation or as a convolution operation. The first method is a commonly used simplification of the diffraction integral. On the other hand, we can also

#99857 - $15.00 USD Received 5 Aug 2008; revised 15 Sep 2008; accepted 22 Sep 2008; published 6 Nov 2008

interpret the diffraction integral as a superposition integral, or in other words, as a convolution operation. This second algorithm allows an effective and economical calculation without any approximation which states that the diffraction integral is calculated using three Fourier transformations through the convolution theorem, that is, $RS(x,y;d)=FT^{-1}\{FT\{U(x,y)\,R(x,y)\}\cdot FT\{h(x,y;d)\}\}$, $RS(x,y)$ being the propagated wave field, $U(x,y)$ the recorded hologram, $R(x,y)$ the reference wave, $h(x,y)$ the impulse response, $(x,y)$ the spatial coordinates, $FT$ the Fourier transform operation and $d$ the propagation distance. The numerical computation of the Fourier transformation operation may be realized with the FFT algorithm.

In this work, we take the advantage of the convolution method. In order to save time in the calculations, we directly define the Fourier transformation of the impulse response: $H(u,v;d)=FT\{h(x,y;d)\}$, where $(u,v)$ are the spatial-frequency coordinates. Moreover, we have used Fresnel approximation in the definition of $H(u,v;d)$. Also, as the different recorded holograms are previously processed to recover the whole set of elementary pupils transmitted using tilted illumination, the calculation of the propagated wave field to an arbitrary distance $d$ is simplified to $RS(x,y;d)=FT^{-1}\{P(u,v)\,H(u,v;d)\}$, where $P(u,v)$ is the recovered frequency band for each recorded hologram. Thus, according to this procedure, it is possible to reconstruct a superresolved wave field of the object by numerically propagating each elementary pupil at different reconstruction distances and by assembling a SA where each propagated pupil is properly placed to its original position at the object's spectrum. The diagram depicted in Fig. 3 shows the whole process for 3-D superresolution imaging.

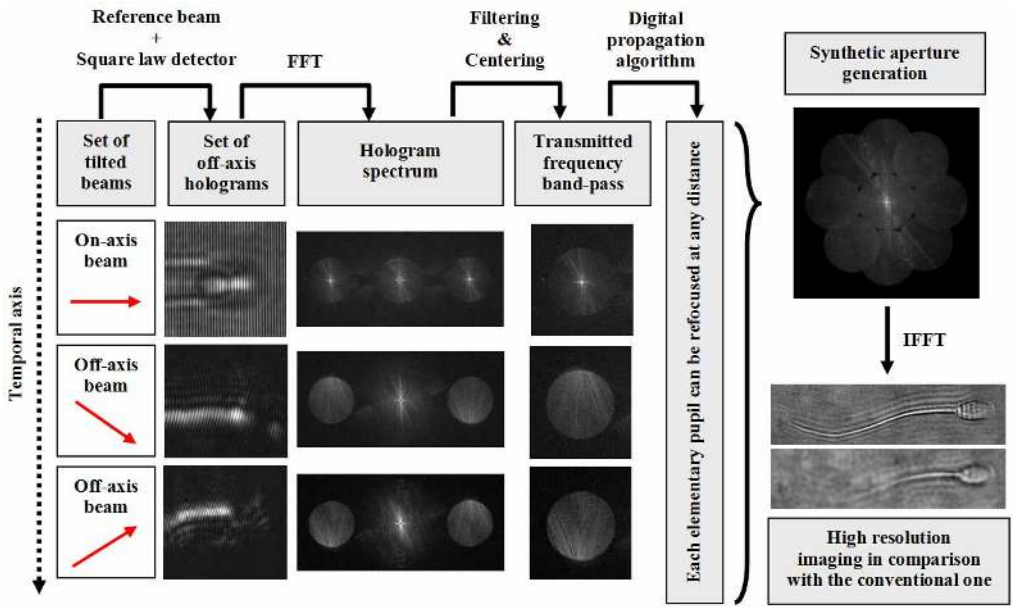


Fig. 3. Schematic chart of the used methodology used where the images depicted in the chart correspond with experimental results obtained with the proposed approach.

But because of each hologram will have different recording phase conditions due to several reasons, three main different phase corrections must be taken into account in order to synthesize a high quality superresolved image. The first one is related with the addition of a global phase to each hologram. This global phase is due to the different optical path travelled for each tilted illumination which is used in the illumination stage. Such optical path difference comes from subwavelength distance mismatches that are impossible to match on each illumination separately. In the second correction we must considered that a difference in the divergence between both interference beams will primarily introduce a misfocus in the image. Thus, although the interferograms are visually matched for equal curvatures in both

#99857 - $15.00 USD Received 5 Aug 2008; revised 15 Sep 2008; accepted 22 Sep 2008; published 6 Nov 2008

beams due to the lens in the reference branch, small errors remains, as visual adjustment cannot go below a mismatch much bellow a wavelength over the full field. This effect is compensated by introducing a quadratic phase factor in the recorded hologram which will be the same for every hologram. And as third correction we find the replacement of each recovered pupil to its original position at the object's spectrum. By knowing the illumination angle (preliminary calibration process), it is possible to add a linear phase factor to the recorded hologram in order to shift each elementary pupil to a rough position in the spatial-frequency domain. A final fine adjustment is achieved by the addition of smaller linear phase factors in both horizontal and vertical directions. Also, this fine tuning process compensates phase variations incoming from misalignments in the optical setup. This procedure is repeated for every elementary pupil considered in the experiment. The full adjustment can be guided by an image quality criterion and automated.

Finally, once the SA has been generated, the superresolved image is obtained by simple inverse Fourier transformation of the information contained in the SA. As a result, we demonstrate full 3-D superresolved imaging on a stack of slice images refocused at incremental depths with the aid of a numerical reconstruction algorithm.

## 4. Experimental results.

As input object we use a swine sperm biosample enclosed in a counting chamber that has a thickness of 16 μm. The unstained sample is dried up allowing fixed sperm cells for the experiments. The sperm cells have a head dimension of 6x9 μm corresponding with the height and width of the ellipsoidal shape of the head, a total length of 55 μm, and a tail's width of 2 μm on the head side and below 1 μm on the end, approximately. As illumination source we use a He-Ne laser (λ=632.8 nm). The illumination grating has a period of 0.83 μm and diffracts the incoming beam at an angle of 49.7º corresponding with its first diffraction order. A commercial medium NA microscope objective (0.42NA Mitutoyo infinity corrected long working distance lens) images the biosample in a plane prior the CCD plane. Notice that the angle defined by the tilted illumination is double the angle that is defined by the NA of the microscope lens (24.8º). So, the generated SA will present a cutoff frequency 3 times higher than the conventional one. The CCD camera (Kappa DC2, 12bits dynamic range, 1352x1014 pixels with 6.7 μm pixel size) records a lensless Fourier hologram in off-axis geometry corresponding with the addition of the object wavefront and a reference beam in oblique incidence. Figure 4 depicts both the recorded holograms and their Fourier transformation corresponding with 3 different illumination cases: on-axis [(a) and (d)], vertical off-axis [(b) and (e)] and oblique off-axis [(c) and (f)]. Magnified areas in (a)-(b)-(c) cases show the fringes in the holograms.

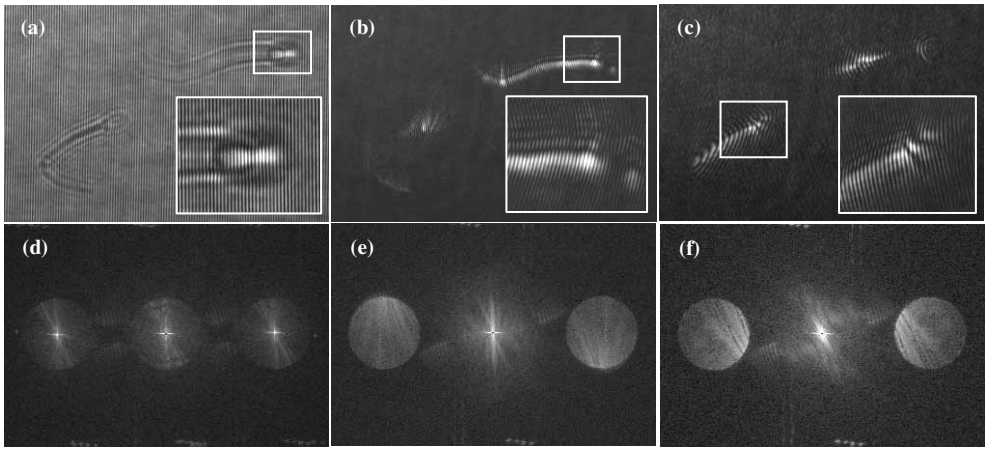


Fig. 4. Examples of three different off-axis recorded holograms and their Fourier transformations corresponding with on-axis illumination [(a) and (d)] and tilted illumination: vertical [(b) and (e)] and oblique [(c) and (f)].

#99857 - $15.00 USD Received 5 Aug 2008; revised 15 Sep 2008; accepted 22 Sep 2008; published 6 Nov 2008

Once the 9 holograms (one on-axis plus 8 off-axis) are recorded and stored in the computer memory, we perform digital processing according to the explanations provided in Section 3. This fact allows the definition of a SA for every propagation distance. Figure 5 depicts one of such SAs. We can see as the SA defines a spectral extension that triples the conventional one. In addition and in agreement with the theoretical predictions, the synthetic numerical aperture (SNA) corresponding with the generated SA that is achieved using the proposed approach is expanded according to the following definition: $SNA=NA_{illum}+NA_{lens}$, where $NA_{illum}$ represents the numerical aperture of the tilted illumination and $NA_{lens}$ is the numerical aperture of the microscope objective (0.42NA). In that sense, a 1.2 SNA, approximately, is achieved.

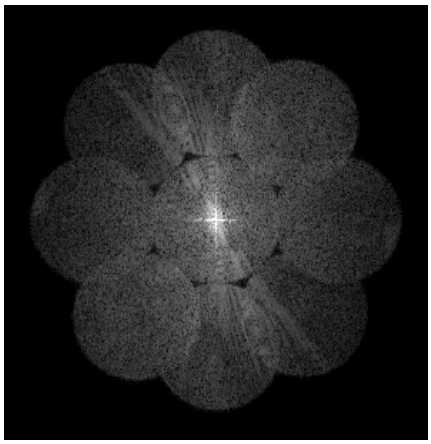

Fig. 5. Generated SA for a given propagation distance.

After that, a superresolved image can be recovered by inverse Fourier transforming the information contained in the generated SA. Figure 6 shows a sequence of images corresponding to different propagation distances in the numerical reconstruction while comparing the conventional images (left column) with the superresolved ones (right column). Cases (a) and (e) correspond with the start of video movies named as (Media 1) and (Media 2) respectively, showing the refocusing ability of the proposed approach. The dashed white line rectangles in cases (b) and (f) magnifies the upper focused cell where the tail's sperm cell that is not visible under conventional illumination [case (b)] becomes resolved using the proposed approach [case (f)], and the neck of the sperm cell is clearly superresolved in case (f).

In a similar way, cases (d) and (h) image the focusing of the other sperm cell placed at a different section in the counting chamber. Also magnified area marked with a dotted white line rectangle depicts a dust particle which is not appreciable under conventional illumination (it seems to be a deformity of the tail's sperm) and that appears clearly visible in the superresolution imaging. Moreover, different residual artifacts start to be visible in the superresolved image [marked with white arrows in case (h)]. These particles are probably due to a dirty chamber and/or coming from the swine semen itself. This effect can be seen in a clearest way in the video movie (Media 2) because the image presented in Fig. 6(h) represents the focusing of the sperm cell while the artifacts become focused at a slightly different distance.

According to the theoretical definition provided by the Rayleigh criterion, the microscope objective has a resolution spot size of 1.84 μm which is not enough to image the tail's narrower part of the sperm cells [magnified areas in Figs. 6(b) and (f)]. After applying the proposed approach, the resolution spot size is reduced until 0.64 μm (corresponding with the theoretically achieved SNA value) and the whole sperm cell is resolved [Fig. 6(f) and (h)]. This fact means a resolution gain factor close to 3.

#99857 - $15.00 USD Received 5 Aug 2008; revised 15 Sep 2008; accepted 22 Sep 2008; published 6 Nov 2008

Also as part of the experimental validation in the resolution improvement, Figure 7 plots the cross sections in the tail's sperm along the solid black lines included in the magnified areas depicted in Figs. 6(b) and (f). We can see as under conventional imaging mode (solid line) the width of the tail's sperm (distance between the two minimums in the solid plot) approaches the theoretical resolution limit (1.84 μm according to the Rayleigh criterion) while this width is reduced below 1 μm for the superresolved case (0.8 μm approximately). Here the resolution gain factor is 2.3, approximately, instead of 3 (the theoretical gain). This discrepancy is due to the finite size of the tail's width, comparable to the resolution spot size, that adds to both measured widths.

## 5. Conclusions.

In summary, by using a digital holographic microscope standard configuration in transmission mode and considering time multiplexing tilted beam illumination onto the input plane, we have demonstrated that it is possible to reconstruct a superresolved wave field of the static input sample for arbitrary reconstruction distances. The resulting complex optical field recovered after filtering and centering process of each transmitted frequency band-pass is used to refocus the complex optical amplitude field on parallels planes. After the definition of a synthetic aperture, the approach yields a super resolved imaging of the 3-D volume of the sample. As the information needed to perform the refocusing is recorded on a single out-of-focus hologram on the CCD plane, there is no need of axial mechanical scanning to extract the 3-D information of the sample. Moreover, as the full information on the optical field diffracted by the sample is recorded, it is possible to process the images as given in standard optical microscopy techniques such as phase-contrast imaging and differential interference contrast imaging. Indeed, also a superresolved quantitative phase imaging is possible by 3-D representation of the unwrapped phase distribution.

The proposed approach has been experimentally validated using a medium NA microscope lens. According with the theoretical definition, the achieved SNA surpasses the limit of air-immersed imaging systems under coherent illumination (NA=1) and it is close to the one for oil immersion imaging methods. Nevertheless, there is no limitation to achieve higher SNA by using a high NA lens and suitable illumination grating. In that sense, the proposed approach will be only limited by the practical theoretical limit of the imaging systems in air, that is, 2 SNA which corresponds to incident illumination beam at quasi-grazing incidence ($NA_{illum} \cong 1$) and diffraction in the backward direction ($NA_{lens} \cong 1$).

#99857 - $15.00 USD Received 5 Aug 2008; revised 15 Sep 2008; accepted 22 Sep 2008; published 6 Nov 2008

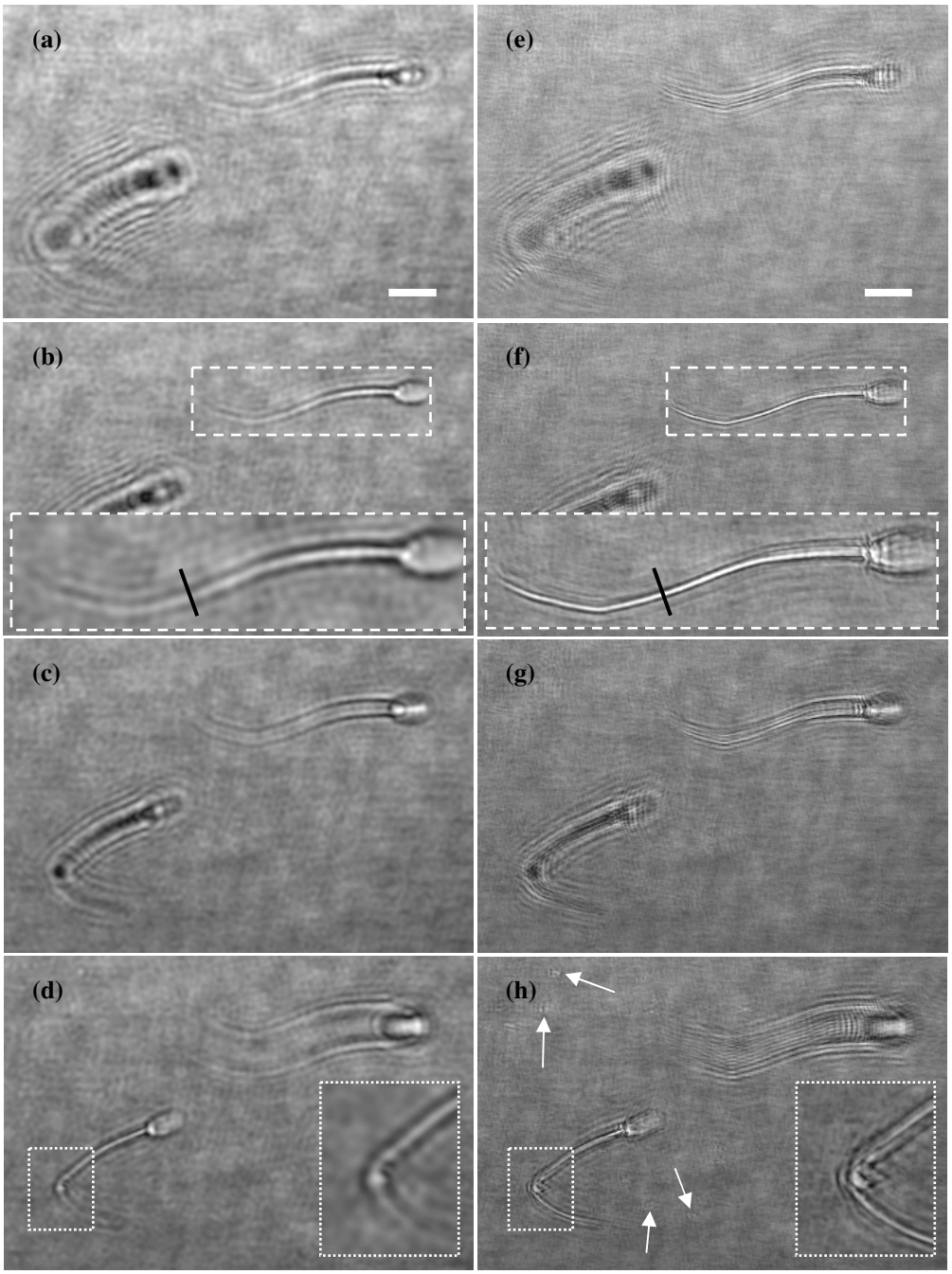


Fig. 6. Image sequence when considering propagation at arbitrary distances for conventional imaging mode (left column) and imaging using the proposed approach (right column). (Media 1) and (Media 2) start with cases (a) and (e) and represent the focusing sequence of low resolution and superresolved imaging, respectively. Scale bars in cases (a) and (e) are 10 μm.

#99857 - $15.00 USD Received 5 Aug 2008; revised 15 Sep 2008; accepted 22 Sep 2008; published 6 Nov 2008

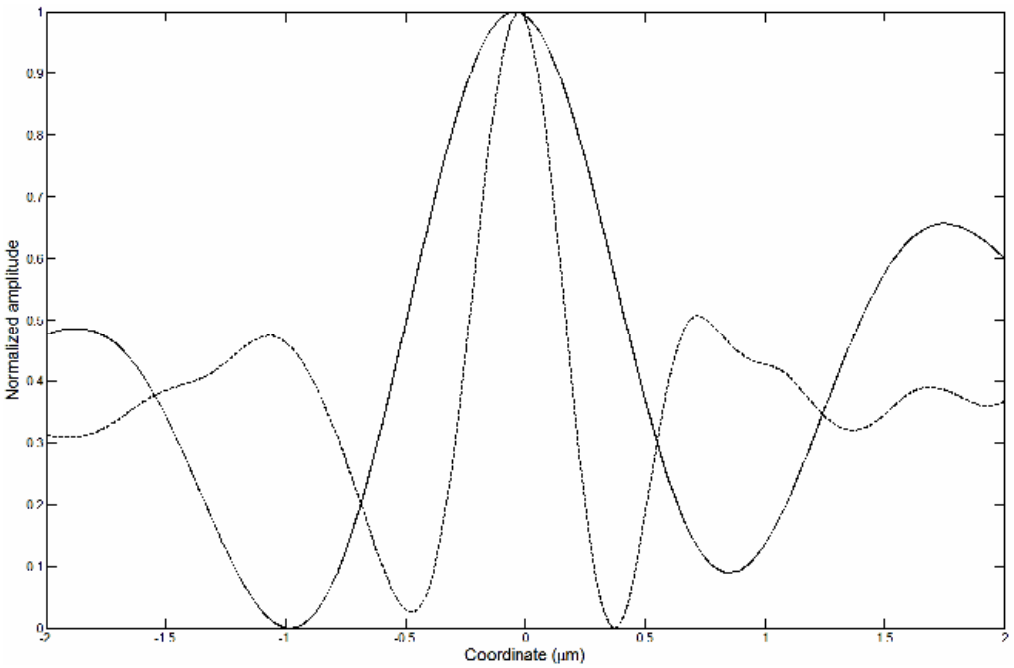


Fig. 7. Comparison between tail sperm cross sections corresponding with conventional imaging mode (solid plot) and applying the proposed approach (dashed plot). Horizontal axis corresponds with linear distance in μm.

**Acknowledgments**

The authors want to thank Prof. Carles Soler and Paco Blasco from Proiser R+D S.L. for providing the swine sperm sample. Also, part of this work was supported by the Spanish Ministerio de Educación y Ciencia under the project FIS2007-60626. Zeev Zalevsky acknowledges the support provided to this work by the Israeli Ministry of Science and Technology in grant # 1958755.

#99857 - $15.00 USD Received 5 Aug 2008; revised 15 Sep 2008; accepted 22 Sep 2008; published 6 Nov 2008